

# Five-year Monitorings of TeV Blazars with *ASCA* and *RXTE*

J.Kataoka,<sup>1</sup> T.Takahashi,<sup>2</sup> F.Takahara,<sup>3</sup> P.G.Edwards,<sup>2</sup> K.Hayashida,<sup>3</sup> S.Inoue,<sup>4</sup>  
N.Iyomoto,<sup>2</sup> N.Kawai,<sup>1</sup> G.M.Madejski,<sup>5</sup> C.Tanihata,<sup>2</sup> and S.J.Wagner,<sup>6</sup>

<sup>1</sup> Department of Physics, Faculty of Science, Tokyo Institute of Technology, Tokyo, Japan

<sup>2</sup> Institute of Space and Astronautical Science, Kanagawa 229-8510, Japan

<sup>3</sup> Department of Earth and Space Science, Osaka University, Osaka, Japan

<sup>4</sup> Theoretical Astrophysics Division, National Astronomical Observatory, Tokyo, Japan

<sup>5</sup> Stanford Linear Accelerator Center, California, USA

<sup>6</sup> Landessternwarte Heidelberg, Königstuhl, Heidelberg, Germany

*E-mail*(JK): kataoka@hp.phys.titech.ac.jp

## ABSTRACT

We study the temporal/spectral variability of two extragalactic TeV sources, Mrk 421 and Mrk 501, based on 5-year observations with the *ASCA* and *RXTE* satellites. We found that the peak of the synchrotron emission exists just in the X-ray band and its position shifted from lower to higher energy when the source became brighter. Relationship between the peak energy and peak luminosity showed quite different behavior in the two sources; Mrk 421 showed very little change in the peak position (0.5–2 keV), while Mrk 501 revealed the largest shift ever observed in blazars (1–100 keV). We analyze these X-ray data with the flux changes in TeV band, which are obtained from 35 *truly* simultaneous observations. Very different spectral evolution of both objects indicates some differences in the electron acceleration mechanism at work during the flares. We argue that the flux variability of Mrk 421 is associated with an increase in the number of electrons, while the flare of Mrk 501 is mostly due to the large changes in maximum energy of electrons. We also discuss the characteristic temporal variability of TeV sources, and implications for the X-ray emitting site in the relativistic jet.

KEY WORDS: blazars: time variability — spectrum: evolution

## 1. Introduction

Blazars, a subclass of AGNs, have outstanding properties in several aspects. They exhibit the most rapid and the largest amplitude variations of all AGNs. Recent observations with the EGRET instrument on-board the *Compton Gamma-Ray Observatory* (*CGRO*) reveal that more than 60 AGNs are bright  $\gamma$ -ray emitters (e.g., Hartman et al. 1999). Remarkably, most of AGNs detected by EGRET were classified as blazars. Observations with ground-based Cherenkov telescopes further confirmed  $\gamma$ -ray emission extending up to TeV energies for a number of nearby blazars.

Overall spectra of blazars (plotted as  $\nu F_\nu$ ) have at least two pronounced continuum components: one peaking between IR and X-rays, and another in the  $\gamma$ -ray regime (e.g., von Montigny et al. 1995). The strong polarization observed in the radio and optical bands (Angel & Stockman 1980) implies that the lower energy component is produced by synchrotron radiation of relativistic electrons in magnetic fields, while inverse-Compton scattering by the same electrons is dominant process

responsible for the high energy  $\gamma$ -ray emission (Ulrich, Maraschi, & Urry 1997). This non-thermal radiation is thought to be emitted in a relativistic jet pointing close to our line of sight (e.g., Urry & Padovani 1995).

Multi-frequency spectra of blazars indicate their variety. There are indications that particles are accelerated more efficiently in blazars having lower luminosities (e.g., Ghisellini et al. 1998). In fact, the luminosity of TeV blazars is the *lowest* end of EGRET detected blazars, while the emission peaks are located at the *highest* frequencies. In low luminosity objects, energy loss by radiation would not be effective because there are less ambient photons to be Compton scattered to higher energies. Thus the TeV blazars gives an important opportunity to study the particle acceleration in blazar jets.

Mrk 421 and Mrk 501 are the proto-type of TeV  $\gamma$ -ray emitting blazars. The first multi-frequency campaign of Mrk 421 including TeV energies was conducted in 1994 (Macomb et al. 1995; Takahashi et al. 1996). The contemporaneous observations implied correlated variability between the keV X-ray and TeV  $\gamma$ -ray emission, while the GeV flux and the radio to UV fluxes showed less vari-

ability. The results from this campaign are important because it suggested the possibility that a single electron population is responsible for both the X-rays and TeV  $\gamma$ -rays, qualitatively agreeing with the Synchrotron self-Compton (SSC) scenario. However, the fact that the X-ray and TeV observations were separated by one day, could introduce uncertainties to draw concrete pictures. Simultaneous, uninterrupted observations are crucial to understand the blazar phenomenon.

In this paper we intensively study Mrk 421 and Mrk 501, with an emphasis on the observations with the X-ray satellites *ASCA* and *RXTE*. Unlike most of the previous work which focused on the photon spectral properties and/or classification of blazars, we also study the rapid time variability and spectral evolution in blazars. The time variability gives us important constraints on the dynamics operating in blazar jets, such as the acceleration, radiative cooling and particle escape. Taking the VLBI observations of superluminal motion into account, we discuss the internal jet structure and emission site in the jet.

## 2. X-ray Observations and Data Analysis

### 2.1. Observations

Mrk 421 and Mrk 501 were observed a number of times with the X-ray satellites *ASCA* and/or *RXTE*. *ASCA* observed Mrk 421 five times with a net exposure of 546 ksec between 1993 and 1998. In the 1998 observation, the source was in a very active state and was detected at its highest-ever level (Takahashi et al. 2000). *RXTE* observed Mrk 501 more than 100 times with a net exposure of 700 ksec between 1996 and 1998. Mrk 501 was in a historical high-state in 1997 (Catanese et al. 1997; Pian et al. 1998; Lamer & Wagner 1999). Multi-wavelength campaigns, including a number of ToO (Target of Opportunity) observations, were conducted during this high state. Observation logs are given in Table 1.

Table 1. Observation log of Mrk 421 and Mrk 501

Source	Satellite	Obs. Time(UT)	Exp. (ksec)	ID
Mrk 421	<i>ASCA</i>	93.05.10 – 05.11	43	(a)
	<i>ASCA</i>	94.05.16 – 05.17	39	(b)
	<i>ASCA</i>	95.04.25 – 05.08	91	(c)
	<i>ASCA</i>	97.04.29 – 05.06	70	(d)
	<i>ASCA</i>	98.04.23 – 04.30	280	(e)
Mrk 501	<i>RXTE</i>	97.04.03 – 04.16	36	(f)
	<i>RXTE</i>	97.05.02 – 05.15	51	(g)
	<i>RXTE</i>	97.07.11 – 07.16	38	(h)
	<i>RXTE</i>	98.02.25 – 10.02	568	(i)

### 2.2. X-ray Time Variability

Figure 1 shows the long-term variation of fluxes, with both *ASCA* and *RXTE* observations plotted. *ASCA* observations of Mrk 421 spanned more than 5 years (from 1993 to 1998), and show that the source exhibits variability by more than an order of magnitude. Blow-ups of the light curves taken in 1995 and 1997 are given in the lower panel (Figure 1 (c),(d)). For Mrk 501, we plot the *RXTE* data because the observations were conducted much more frequently than the *ASCA* observations. The *RXTE* observations spanned more than 3 years and significant flux changes are clearly detected. Blow-ups of light curves are given in Figure 1 (f)–(h).

To evaluate variability features in blazars, we examine the use of a numerical technique called the structure function (hereafter, SF). While in theory the SF is completely equivalent to traditional Fourier analysis methods, it has several significant advantages. Firstly, it is much easier to calculate. Secondly, the SF is less affected by gaps in the light curves. The definitions of SFs and their properties are given by Simonetti et al. (1985). The first order SF is defined as

$$\text{SF}(\tau) = \frac{1}{N} \sum [a(t) - a(t + \tau)]^2, \quad (1)$$

where  $a(t)$  is a point of the time series (light curves)  $\{a\}$  and the summation is made over all pairs separated in time by  $\tau$ .  $N$  is the number of such pairs.

The structure functions calculated from the light curves (Figure 1) are given in Figure 2. The SFs are normalized by the square of the mean fluxes, and are binned at logarithmically equal intervals. Both the SFs show a rapid increase up to  $\tau/\text{day} \simeq 1$ , then gradually flatten to the observed longest time-scale of  $\tau/\text{day} \geq 1000$ . Fluctuations at large  $\tau$  ( $\tau/\text{day} \geq 10$ ) are due to the extremely sparse sampling of data. In order to demonstrate the uncertainties caused by such sparse sampling, and to firmly establish the reality of the “roll-over”, we simulated the long-term light curves following the *forward method* described in Iyomoto (1999). We found that (1) the PSD of the TeV sources have at least one roll-over at  $10^{-6}$  Hz  $\leq f_{\text{br}} \leq 10^{-5}$  Hz ( $1 \leq \tau/\text{day} \leq 10$ ), and (2) the PSD changes its slope from  $\propto f^{-1 \sim -2}$  ( $f < f_{\text{br}}$ ) to  $\propto f^{-2 \sim -3}$  ( $f > f_{\text{br}}$ ) around the roll-over (Kataoka et al. 2001a).

### 2.3. X-ray Spectral Evolution

We next performed model fitting to evaluate the X-ray photon spectra of Mrk 421 and Mrk 501. In general, the photon spectra of TeV sources show convex shape, where the model with a single power law functions plus absorption arising from neutral material could not fit the observed spectra. We thus use another model which is expected to fit the spectrum

$$\frac{dN}{dE} = N_0 \times \exp(-N_{\text{H}}^{\text{Gal}} \sigma(E)) E^{-\Gamma} \times \exp(-E_c/E), \quad (2)$$

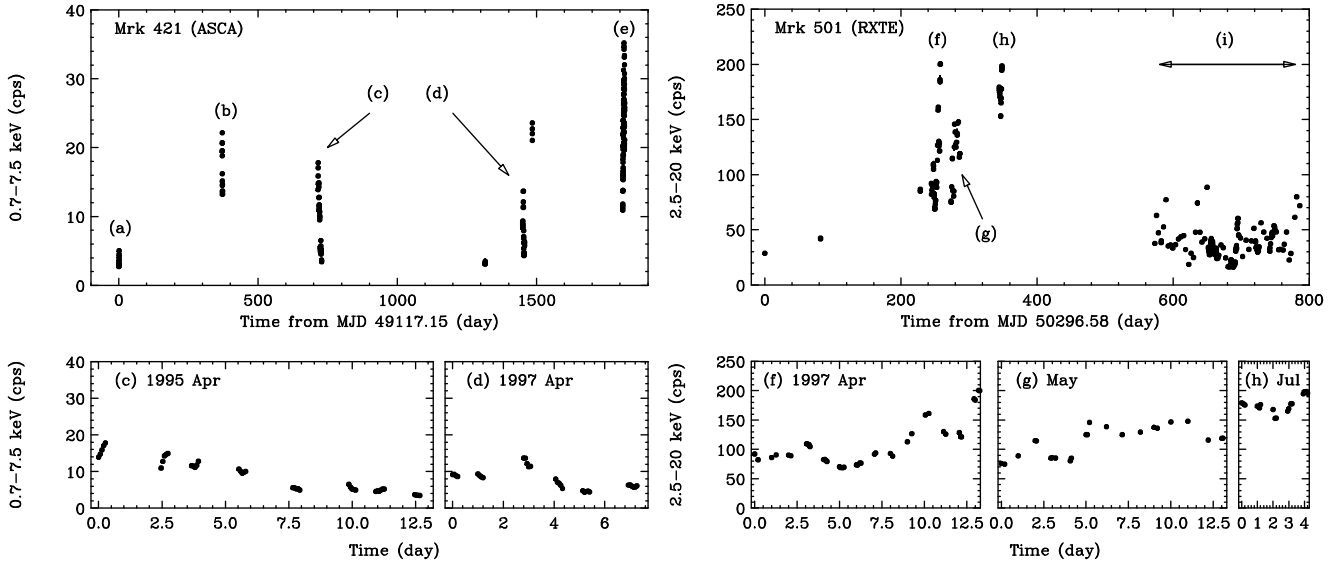


Fig. 1. Long-term flux variation of Mrk 421 (*left*) and Mrk 501 (*right*)

where  $\Gamma$  is the photon index and  $E_c$  is the cutoff energy, respectively. Using this relatively simple model, one can differentiate the function analytically. The peak energy  $E_p$  in  $\nu F_\nu$  are given  $E_p = \frac{E_c}{\Gamma-2}$ . We cannot determine  $E_p$  for  $\Gamma \leq 2$ , because in such cases, the spectra are monotonously rising in the total energy band.

We divided the observations into 5 msec exposure segments and fitted the photon spectra for individual segments. In this case, statistically acceptable fits were obtained. The distribution of peak luminosity  $L_p$  versus peak energy  $E_p$  is summarized in Figure 3. The peak luminosity is simply calculated from the luminosity at  $E = E_p$ . Mrk 421 shows very modest shifts in the peak position. A clear correlation between the peak energy  $E_p$  and the peak luminosity  $L_p$  was detected for the first time for both Mrk 421 and Mrk 501:  $E_p \propto L_p^{0.4}$  for Mrk 421 and  $E_p \propto L_p^{1.6}$  for the case of Mrk 501. Extrapolating the relation between  $E_p$  and  $L_p$ , we expect that synchrotron peak reaches to  $\sim 100$  keV in the high state of Mrk 501, which is the largest shift ever observed in blazars (Pian et al. 1998; Kataoka et al. 1999).

### 3. Multi-frequency Analysis

In previous sections, we have investigated the rapid variability and spectral evolution of TeV blazars, highlighting the X-ray observations by *ASCA* and *RXTE*. However, the overall spectral energy distribution of blazars generally ranges over a very wide range – from radio to TeV  $\gamma$ -ray bands – and such spectra are one of the most important features allowing us to understand these sources. To reveal the multi-frequency properties of TeV blazars, we have to carry out multi-frequency monitoring campaigns of the source in various states of activity.

Results from previous campaigns strongly suggest correlated variations in X-ray and TeV  $\gamma$ -ray fluxes, while variability is much less pronounced in other energy bands. However, a problem remains that most of the data are taken either *non-simultaneously* or are very sparsely sampled (e.g., Macomb et al. 1995; Buckley et al. 1996). The discussion based on those *quasi-simultaneous* data may be incomplete. We need *exactly* simultaneous monitoring, especially in the X-ray and TeV energy bands, to correctly understand the sources. In the following, we summarize the results from *truly* simultaneous campaigns of TeV blazars conducted from 1996 to 1998.

Evolution of multi-frequency spectrum of Mrk 421 is shown in Figure 4(*left*). Open circles come from Macomb et al (1995), while other symbols represent our new results taken exactly simultaneously in X-ray (also *EUVE*) and TeV  $\gamma$ -ray bands. Several important features are seen in the figure. First, a clear correlation can be seen between the keV X-ray flux and the TeV  $\gamma$ -ray fluxes. The amplitude of TeV flux variation is less or almost comparable with that in the X-ray energy bands. Detailed analysis showed that the correlation is expressed as  $[\text{TeV } \gamma\text{-ray flux}] \propto [\text{X-ray flux}]^{0.92 \pm 0.12}$ . Second, the slope of X-ray photon spectra ( $\Gamma_{\text{X-ray}} \sim 3$ ) are steep, and very similar to those in the TeV energy band ( $\Gamma_{\text{TeV}} \sim 3$ ; Aharonian et al. 1999b). Third, although X-ray flux changed dramatically in various seasons, only small changes are implied in the synchrotron peak position, as we have quantitatively discussed in § 2.3.

Evolution of the multi-frequency spectrum of Mrk 501 is shown in Figure 4 (*right*). Open circles are data from public archive (taken from Kataoka et al. 1999), while

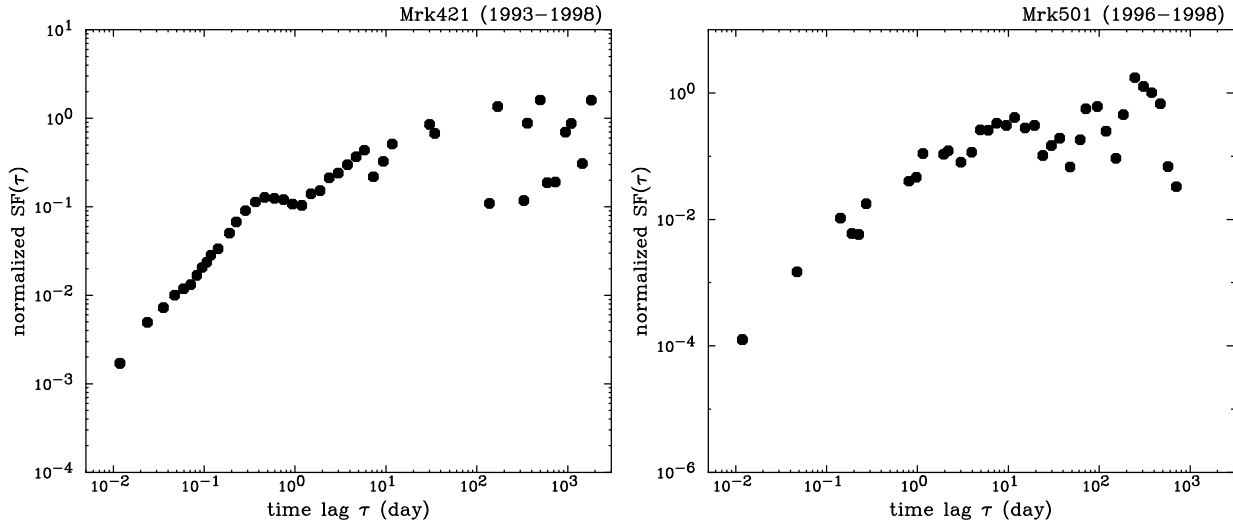


Fig. 2. Structure functions of Mrk 421 (*left*) and Mrk 501 (*right*)

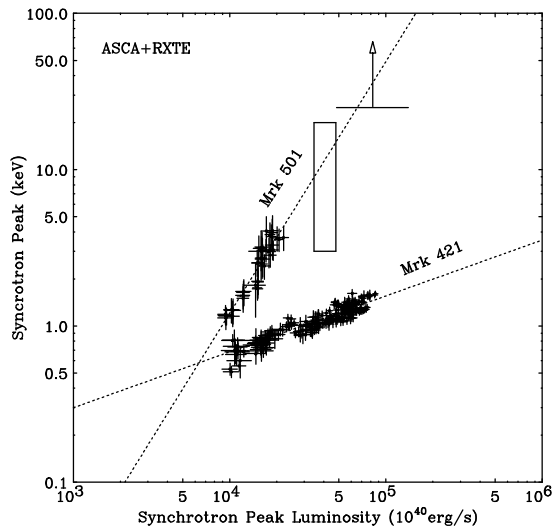


Fig. 3. Distribution of peak luminosity  $L_p$  versus peak energy  $E_p$

other symbols represent our new results derived from simultaneous monitoring in the X-ray and TeV  $\gamma$ -ray bands. For the data obtained in March 1996, we also plot the EGRET and optical data. Compared to the results for Mrk 421, some significant differences are implied in the multiband spectra. First, the changes in X-ray flux are accompanied by large shift in the position of the synchrotron peak. Second, the slope of X-ray spectra ( $\Gamma$ ) varies widely, ranging from  $\Gamma_{X\text{-ray}} \sim 1.7$  to 2.5, while the photon index in the TeV energy band is almost unchanged;  $\Gamma_{\text{TeV}} \sim 2.5$  (e.g. Aharonian et al. 1999a). Third, amplitude of TeV flux variation is much larger than that in the X-ray energy band. The correlation between two energy bands is expressed as  $[\text{TeV } \gamma\text{-ray flux}] \propto [\text{X-ray flux}]^{1.96 \pm 0.07}$ .

#### 4. Discussion: what can we learn?

As first pointed out by Kataoka (2000), the little power of rapid variability ( $\leq 1$  day) in TeV sources provides important clues to the X-ray emitting site in the jet. The characteristic time-scale of each flare event  $t_{\text{var}} \geq 1$  day should reflect the size of the emission region, which we infer to be  $\geq 10^{16} (\Gamma/10)$  cm in the source co-moving frame, if emitting blobs are approaching with Lorentz factors  $\Gamma$  ( $\Gamma \simeq 10$ ; Vermeulen & Cohen 1994). This range of Lorentz factors is independently inferred from constraints that can be derived from the spectral shape and variability of TeV blazars (e.g., Tavecchio, Maraschi and Ghisellini 1998; Kataoka et al. 1999).

If the jet is collimated to within a cone of constant opening angle  $\theta \simeq 1/\Gamma$  and the line-of-sight extent of

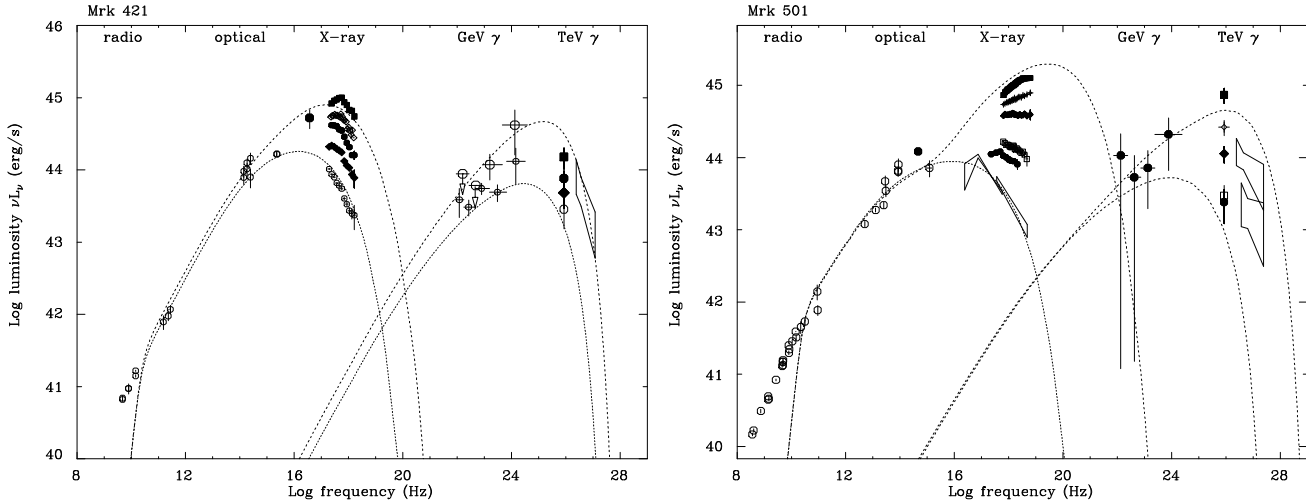


Fig. 4. Evolutions of multi-frequency spectra : Mrk 421 (*left*) and Mrk 501 (*right*). Dotted line represents the best fit SSC model for the quiescent/flare state. Figure from Kataoka et al. (2001b).

shock is comparable with the angular extent of the jet, one expects that the X-ray emission site is located at distances  $D \geq 10^{17} (\Gamma/10)^2$  cm from the base of the jet. Only little variability shorter than  $t_{\text{var}}$  strongly suggests that no significant X-ray emission can occur in regions closer than this to the black hole. The relativistic electrons responsible for the X-ray emission are most likely accelerated and injected at shock fronts occurring in the jet (e.g., Inoue & Takahara 1996). The lack of short term variability may then imply that shocks are nearly absent until distances of  $D \geq 10^{17} (\Gamma/10)^2$  cm. Further discussion of the characteristic timescale is given in Kataoka et al. (2001a), which also suggests a possible link between the jet and the central engine.

In § 2.3, we found that the position of the synchrotron peak shifts from lower to higher energy when the source becomes brighter. The difference of spectral evolution in Mrk 421 and Mrk 501 implies that quite different mechanisms were at work when the sources went into the flaring states. Since the peak luminosity is proportional to the number of photons at peak ( $n_{\text{ph}}(E_p)$ ) multiplied by the peak energy, a simple relation can be found:

$$L_p \propto E_p n_{\text{ph}}(E_p) \propto \gamma_p^2 n_e(\gamma_p), \quad (3)$$

where  $\gamma_p$  is the Lorentz factor of electron which emits photon of energy  $E_p$  and  $n_e(\gamma_p)$  is the number of electrons at  $\gamma_p$ . We thus find the relations,

$$n_e(\gamma_p) \propto \gamma_p^{3.6} \quad (\text{Mrk421}), \quad (4)$$

$$n_e(\gamma_p) \propto \gamma_p^{-0.8} \quad (\text{Mrk501}). \quad (5)$$

This implies that for the case of Mrk 421, increase of  $\gamma_p$  by a factor of 2 requires more than factor 10 *increase* in number of electrons at peak energy. On the other hand,

the same amount of increase of  $\gamma_p$  requires *decreases* in number of electrons by a factor of 2 for the case of Mrk 501. Such variations in spectral behaviors may be associated with the difference of physical conditions in relativistic jets, which is discussed below. Full descriptions are given in Kataoka (2000) and Kataoka et al. (2001b).

Assume that a substantial amount of gas (e.g., in a form of clouds) is distributed in the jet. In these clouds, density of low-energy electrons is enhanced as compared to the ambient, but other physical quantities such as magnetic field strength are unchanged. Those clouds essentially provide a plentiful source of low-energy electrons for the shock front. When a shock front overruns one of such clouds, fresh electrons are successively injected and assumed to undergo continuous acceleration by repeatedly crossing and recrossing the shock front, as well as simultaneously cooling by synchrotron radiation (e.g., Kirk, Rieger & Mastichiadis 1998). In this scenario, number of electrons increases significantly, but only small changes are implied for the maximum Lorentz factor as were observed in Mrk 421.

On the other hand, when clouds are absent or very sparsely distributed in the jet, flares may be produced in several different manners. For example, if the shock overruns the enhanced tangled-magnetic field region, this may cause changes in acceleration time of electrons, and hence increase the maximum Lorentz factor. Importantly, regardless of detailed models for flaring behaviour, total number of electrons is *conserved* in this case. During the flare, acceleration can be assumed to be more efficient than radiative cooling, thus the present electron population as a whole will be accelerated to higher energies, but no additional electrons are supplied

into the shock.

In latter case, numbers of electrons at the peak ( $n_e(\gamma_p)$ ) will *decrease*, reflecting the power-law shape of an electron population. If the differential number density of electrons is expressed as  $N_e \propto \gamma^{-2}$  (standard shock), electron number decreases as  $n_e(\gamma_p) \propto \gamma_p N_e(\gamma_p) \propto \gamma_p^{-1}$ . Importantly, this relation is very close to the case we have observed in Mrk 501.

Present discussion based on the X-ray spectral evolution suggests very important implications for internal jet structures. Only a small shift of synchrotron peak observed in Mrk 421 may be associated with electron clouds *filling* the jet, while the jet of Mrk 501 seems to be relatively empty. During the flare of Mrk 421, kinetic power of the shock is equally distributed to large number of low-energy electrons newly injected into the shock, thus increasing the number of high energy electrons. Large shifts of synchrotron peak observed in Mrk 501, on the other hand, is possible only when the internal jet is rather sparse and transparent to the shock propagation. Kinetic power of the shock is spent to *increase* the energies of individual electrons and hence *number-conservative*.

It may thus be worthwhile to compare our X-ray implications to the VLBI results. Accurate measurements of changes in the parsec-scale jet structure imaged with VLBI provide constraints on the jet kinematics and geometry. When combined with estimates of the Doppler beaming factor (determined, for example, from the X-ray time variability), the apparent motion of the jet components can be used to constrain the Lorentz factor of the jet and the angle of the jet to the line-of-sight. Although VLBI observations do not yet have an enough resolution to image the region production of the X-ray/ $\gamma$ -rays ( $\sim 0.01$  pc), they provide the highest resolution structural information available, and can image the region immediately downstream.

Mrk 421 and Mrk 501 are observed in a space VLBI project using the *HALCA* satellite and 12 ground stations. It is interesting that the subparsec- and parsec-scale jets of Mrk 421 and Mrk 501 appear to be weak relative to those of other blazars (Marscher et al. 1999). Most importantly, superluminal motions have been detected only for Mrk 501 ( $v = 6.7 c$ ; Giovannini et al. 1998), while subluminal motions were implied for Mrk 421 ( $v \simeq 0.3 c$ ; Piner et al. 1999). By assuming that the bulk and pattern jet velocity are comparable, Giovannini et al. (1998) derive that the beaming factor of Mrk 501 as  $\delta \sim 1.3\text{--}5.6$ . For the case of Mrk 421, the results are consistent with *no-beaming*.

In any case, the estimated beaming factors for both sources are relatively low compared with the lower limits derived from time variabilities in other wavebands; for examples, Takahashi et al. (1996) derived  $\delta \geq 5$  for Mrk

421 and Kataoka et al. (1999) derived  $\delta \geq 6$  for Mrk 501 using the X-ray/TeV  $\gamma$ -ray time variability. Marscher (1999) discussed that rather low superluminal apparent speeds and lackluster variability properties of the radio jets evidences that the bulk flow of the jets *decelerates* from X-ray/TeV  $\gamma$ -ray emitting section ( $\sim 0.01$  pc) to the radio emitting region ( $\sim 1$  pc). The weak subparsec- and parsec-scale jets of those objects are readily understood as the consequence of heavy energy and momentum loss in the upstream of the jet where most of the energy and momentum of the relativistic electrons are transferred to the radiation in the X-ray and TeV  $\gamma$ -rays.

Remarkably, very different manners of X-ray spectral evolutions of Mrk 421 and Mrk 501 presented in this paper is exactly consistent with those VLBI observations. Our X-ray observations predict that relativistic outflows of Mrk 421 will be decelerated faster than that for Mrk 501, because the jet of Mrk 421 is filled with low-energy materials and kinetic energy of outflows are more efficiently dissipated during the propagation. The absence of superluminal motion of Mrk 421 in radio bands thus indicates that the high energy outflow has been sufficiently decelerated when it reaches to more distant, radio emitting region.

## References

- Aharonian, F., et al. 1999a, A & A, 349, 29
- Aharonian, F., et al. 1999b, A & A, 350, 757
- Buckley, J. H., et al. 1996, ApJ, 472, L9
- Catanese, M., et al. 1997, ApJ, 487, L143
- Ghisellini, G., et al. 1998, MNRAS, 301, 451
- Giovannini, G., et al. 1998, in the proceedings of “BL Lac phenomenon” Turku, Finland
- Hartman, R. C., et al. 1999, ApJS, 123, 79
- Inoue, S., & Takahara, F. 1996, ApJ, 463, 555
- Iyamoto, N., 1999, Ph.D Thesis, University of Tokyo
- Kataoka, J., et al. 1999, ApJ, 514, 138
- Kataoka, J., 2000, Ph.D Thesis, University of Tokyo
- Kataoka, J., et al. 2001a, ApJ, in press (astro-ph/0105022)
- Kataoka, J., et al. 2001b, submitted
- Kirk, J. G., et al. 1998, A&A, 333, 452
- Lamer, G., & Wagner, S. J. 1998, A & A, 331, L13
- Macomb, D. J., et al. 1995, ApJ, 449, L99
- Marscher, A. P., 1999, Astroparticle Physics, 11, 19
- Pian, E., et al. 1998, ApJ, 492, L17
- Piner, B. G., et al. 1999, ApJ, 525, 176
- Simonetti, J. H., et al. 1985, ApJ, 296, 46
- Takahashi, T., et al. 1996, ApJ, 470, L89
- Takahashi, T., et al. 2000, ApJ, 542, L105
- Tavecchio, F., et al. 1998, ApJ, 509, 608
- Ulrich, M. -H., et al. 1997, ARAA, 35,445
- Urry, C. M., & Padovani, P., 1995, PASP, 715, 803
- Vermeulen, R. C., & Cohen, M. H. 1994, ApJ, 430, 467